Serrano, J.; Navarro, R.; García-Cuevas González, LM.; Inhestern, LB. (2019). Contribution to Tip Leakage Loss Modeling in Radial Turbines Based on 3D Flow Analysis and 1D Characterization. International Journal of Heat and Fluid Flow. 78. https://doi.org/10.1016/j.ijheatfluidflow.2019.108423

Method for Non-Dimensional Tip Leakage Flow Characterization in Radial Turbines

José Ramón Serrano
Professor, Fellow of ASME
Roberto Navarro
Lecturer
Luis Miguel García-Cuevas
Lecturer
Lukas Benjamin Inhestern*
Graduate Student, Student Member of ASME
Email: luin@mot.upv.es
CMT-Motores Térmicos
Universitat Politècnica de València
Valencia 46022, Spain

Tip leakage loss characterization and modeling plays an important role in small size radial turbine research. The momentum of the flow passing through the tip gap is highly related with the tip leakage losses. The ratio of fluid momentum driven by the pressure gradient between suction side and pressure side and the fluid momentum caused by the shroud friction has been widely used to analyze and to compare different sized tip clearances. However, the commonly used number for building this momentum ratio lacks some variables, as the blade tip geometry data and the viscosity of the used fluid. To allow the comparison between different sized turbocharger turbine tip gaps, work has been put into finding a consistent characterization of radial tip clearance flow. Therefore, a non-dimensional number has been derived from the Navier Stokes Equation. This number can be calculated like the original ratio over the chord length. Using the results of wide range CFD data, the novel tip leakage number has been compared with the traditional and widely used ratio. Furthermore, the novel tip leakage number can be separated into three different non-dimensional factors. First, a factor dependent on the radial dimensions of the tip gap has been found. Second, a factor defined by the viscosity, the blade loading, and the tip width has been identified. Finally, a factor that defines the coupling between both flow phenomena. These factors can further be used to filter the tip gap flow, obtained by CFD, with the influence of friction driven and pressure driven momentum flow.

Nomenclature
Latin Letters

a Fitting constant
b Fitting constant
BSR Blade Speed Ratio
c Fitting constant
CFD Computational Fluid Dynamics
dr Radial integrator
IGV Inlet Guide Vane
i Incidence
l Length
$\dot{m}$ Mass flow
M Momentum
N Rotational speed
NS Based on Navier Stokes equation
PS Pressure side
p Pressure
R Momentum ratio non-dimensional number
Re Reynolds number
SS Suction side
T Temperature
TE Trailing edge
t Total or stagnation conditions
VGT Variable Geometry Turbine
$\dot{W}$ Power
y^+ Nondimensional wall distance

Subscripts
ax. Axial component
eff. Effective
filt. Filtered
fl. Fluid
geom. Geometry
in Inlet
out Outlet

*Address all correspondence for other issues to this author.

red. Reduced numbers
s Static conditions
sh. Shroud
surf. Value on surface
tip Blade tip
turb. Turbine

Greek Letters

α Stator blade angle
β Incidence angle in rot. ref. frame
γ Blade surface angle, isentropic exponent
Δ Difference
∂ Increment
η Efficiency
θ Tangential component
π Corresponding pressure ratio
σ Blade speed ratio
ω Angular velocity
ρ Density
μ Viscosity

Symbols

$+$ Positive direction
$-$ Negative direction
$\bar{}$ Averaged value
$\perp$ Perpendicular

1 Introduction

While turbocharging is commonly used in conventional diesel engines to increase the intake pressure, it is more and more required for downsizing purposes in gasoline engines to meet increasingly tightened exhaust gas restrictions by governments worldwide. In the turbocharging system, the turbine experiences highly unsteady flow conditions in consequence of the pulsating flow generated by the cylinder exhaust of the reciprocating combustion engine. Furthermore, urban driving that gains continuously importance can lead to additional unsteadiness due to acceleration and deceleration of engine and turbocharger axis [1, 2]. Thus, the turbine operates most of the times under off-design conditions [3] where the overall internal flow is rather unknown. As the turbine is attached to a compressor that acts as a brake with a very limited braking torque range at any given rotational speed it is difficult to obtain measurements under these off-design conditions. However experimental procedures have been developed to measure in this zone [4, 5, 6, 7], extended maps are not commonly available yet. Nevertheless, various extrapolation models have been published to extrapolate narrow measurement maps [8, 9, 10]. This kind of models often rely on submodels to estimate losses like passage or tip leakage losses.

Due to the typically small size of turbocharger radial turbines, they have rather small blade tip gap to blade tip radius ratios. This makes the turbocharger turbine efficiency especially prone to tip leakage losses as confirmed by Kammeyer et al. [11]. Hence, the modeling of the losses and a detailed knowledge of the main physical effects are of high interest for one dimensional modeling and turbine design. Due to the aforementioned off-design operation of the turbine, models valid over a wide range of operating conditions, from low pressure ratios to high pressure ratios and from low rotational speed to high rotational speed, are in demand. Several one-dimensional models predicting tip leakage losses have been published. The model introduced by Kammeyer et al. [12] is based on an empirical approach and is able to predict efficiency losses at design points dependent on geometrical information as the ratio of the tip gap to the tip width or to the rotor tip radius. In one-dimensional turbocharger turbine modeling the tip leakage loss model presented by Baines [13] is widely used.

Dambach et. al [14, 15, 16] highlighted the importance of pressure driven tip leakage flow and friction driven tip leakage flow, which goes in opposing direction. Researchers, as in [14, 17], stated that the tip leakage related loss can mainly be correlated with the mass and momentum passing through the tip gap. Furthermore, it was shown that the ratio of pressure induced momentum to friction induced momentum can qualitatively predict locations of higher and lower efficiency losses over the tip. However, this rather simple correlation does not own geometrical information, so that important conclusions might be undiscovered.

The consistent modeling of the reciprocal effect of opposing flow patterns in the tip region over wide range of speeds and blade loadings can be challenging. The physical model described in [18] can model tip leakage mass flow and momentum which has further been correlated to obtain tip leakage losses for one-dimensional extrapolation models. While this model also relies on general geometrical information, it uses fitting coefficients to model the complex composition of contrarious fluid flows though the tip gap over a wide range of speeds and pressure ratios. Thus, an estimation for changed geometries before building, measuring and applying the model is not possible yet.

The objective of this paper is to find an aerodynamically based correlation that can predict the momentum ratio of friction and pressure induced flow for changed geometries and for a wide range of operating conditions, that can be used in one dimensional modeling and further analysis. Therefore, the simulated data base has been presented and shortly analyzed. Following, the new correlation for the tip momentum ratio has been derived. Finally, results and possible fields of application are shown.

2 CFD Setup & Validation Results

As data basis for the following analysis CFD results of operating conditions in a wide range have been used [19] and further simulations have been executed. The analyzed turbine is a commonly sized turbocharger turbine with variable stator vanes. The geometrical details have been listed in Tab. 1 and related nomenclature of geometrical parameters have been shown in Fig. 1.

All simulations have been solved with the segregated solver in Star-CCM+ 12.04. Steady RANS simulations have been used where the turbulence has been calculated by kω-SST model [20], which has been recommended for radial

Stator	
Blade number	11
Blade angle α (VGT opening)	62.95° (60 %)
Rotor	
Blade number	9
Inlet radius $r_{tip,in}$	20.05 mm
Outlet radius $r_{tip,out}$	19 mm
Outlet blade angle γ_{out}	59°
Inlet tip clearance $\Delta r_{tip,in}$	0.36 mm
Outlet tip clearance $\Delta r_{tip,out}$	0.4 mm
Axial tip clearance length ($l_{tip,ax.}$)	13 mm
Leading edge thickness $\Delta\theta$	0.0195 rad

Table 1: Turbine geometry

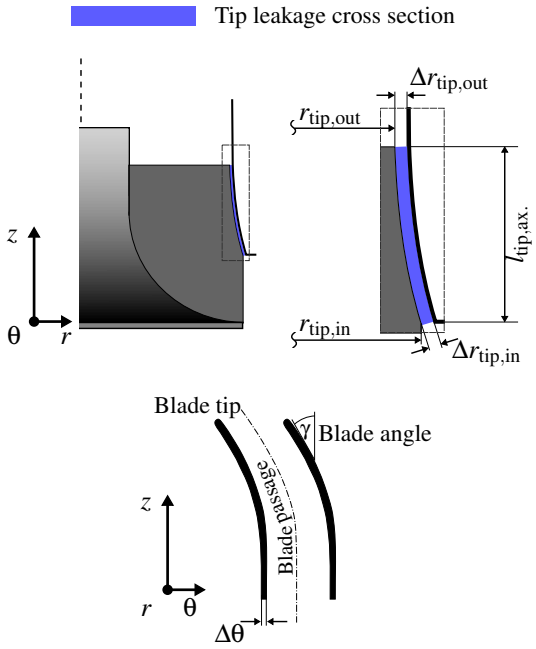

Figure 1: Tip geometry nomenclature

turbocharger simulations [21, 22, 23]. A polyhedral mesh with fine prism layer resolution on the wall has been used to resolve the boundary layer. An overall wall y^+ value of around 1 has been obtained. A detailed mesh analysis, the simulation setup to achieve CFD results at very low pressure ratios and its validation is described in detail in [19]. The mesh convergence in the tip region was analyzed separately by doubling the mesh density without a considerable change in the tip leakage flow mass flow and momentum, which are mainly investigated in this paper.

Simulations have been executed at four different speedlines from a low reduced speed of 1710 rpm/K$^{0.5}$ up to a high reduced speed of 6715 rpm/K$^{0.5}$ while the VGT opening is set to 60 %. Each speedline has been simulated over a wide range to get a complete picture of flow conditions that can occur during transient driving conditions. The line of highest reduced speed has been further calculated with several tip gap geometries. The tip gap height has been increased by 50 % and decreased by 50 % as it can be seen in Fig. 2. The original shroud has been maintained and only the rotor blade has been adjusted for this modification.

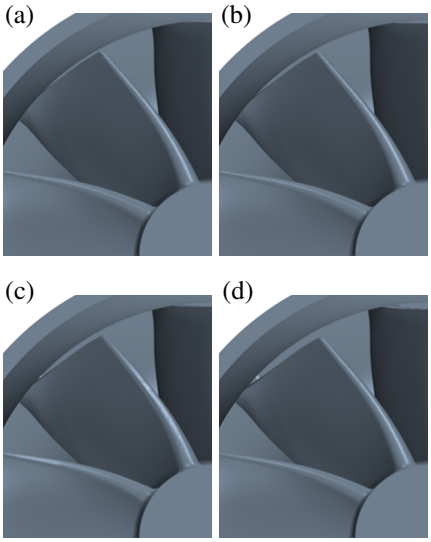

Figure 2: Tip gap geometry variation: (a) 50 % $\Delta r_{tip,ref.}$; (b) 75 % $\Delta r_{tip,ref.}$; (c) 100 % $\Delta r_{tip,ref.}$; (d) 150 % $\Delta r_{tip,ref.}$

Figure 3 and Fig. 4 show simulated turbine efficiency according to Eqn. 1 and reduced turbine mass flow of simulated cases in comparison with experimentally obtained data.

$$\eta = \frac{T_{t,in} - T_{t,out}}{T_{t,in}\left[1 - \left(\frac{1}{\pi}\right)^{\frac{\gamma-1}{\gamma}}\right]} \quad (1)$$

Experimental measurements in an extended range have been realized by using an IGV upstream the inlet of the compressor wheel to convert the compressor into a centrifugal turbine like it has been explained in [6]. This way it was possible to maintain the rotational speed with power produced by the compressor wheel and to measure up to running points where the turbine even consumes energy and thus, owns negative efficiencies as they were reported by other researchers [5, 7, 24].

Experimental variations in the VGT positioning are inherent to the VGT moving mechanism. For the validation

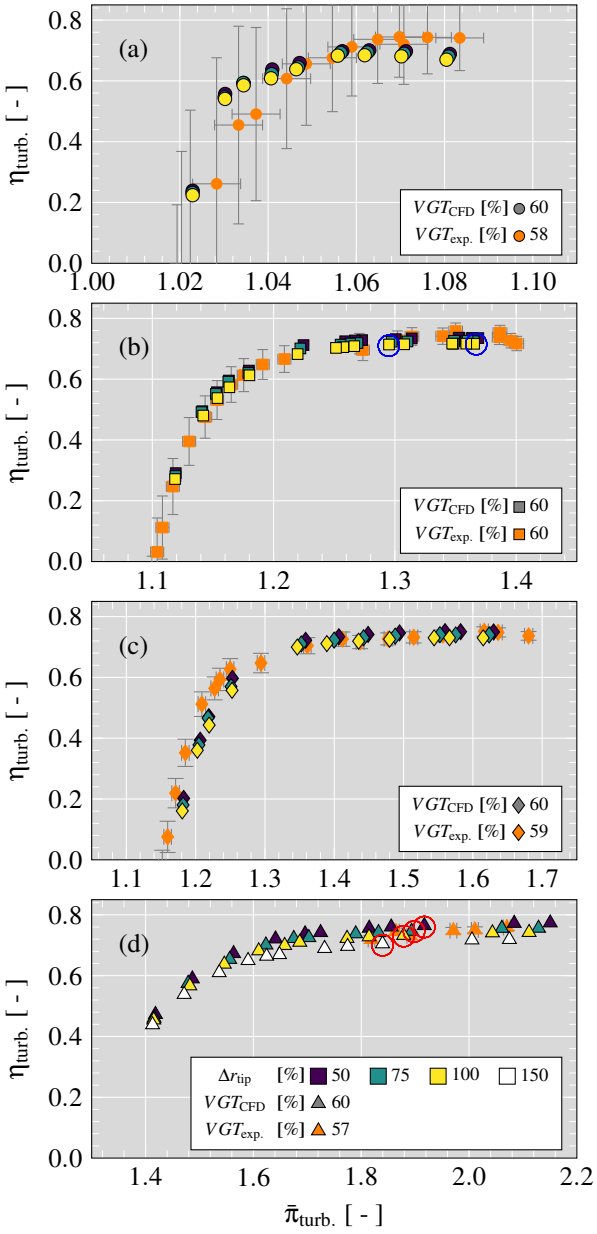

Figure 3: Efficiency of simulated and measured running points at: (a) 1710 rpm/$K^{0.5}$; (b) 3890 rpm/$K^{0.5}$; (c) 4890 rpm/$K^{0.5}$; (d) 6715 rpm/$K^{0.5}$

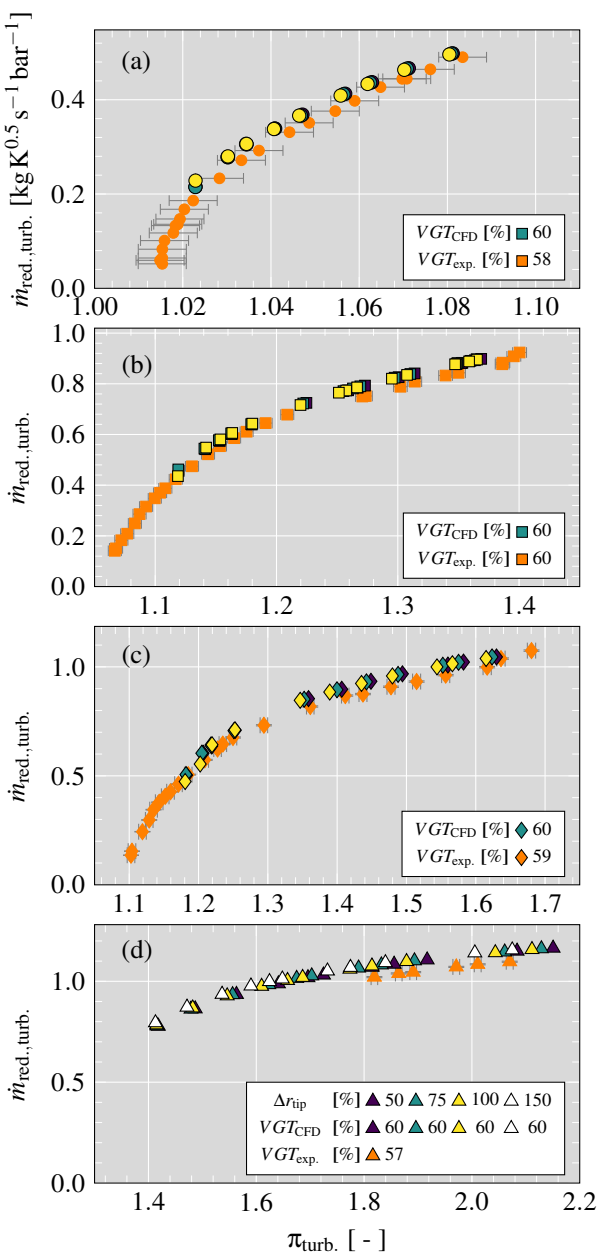

Figure 4: Reduced mass flow of simulated and measured running points at: (a) 1710 rpm/$K^{0.5}$; (b) 3890 rpm/$K^{0.5}$; (c) 4890 rpm/$K^{0.5}$; (d) 6715 rpm/$K^{0.5}$

of the CFD method the VGT opening was stepwise changed until the experimental mass flow was achieved in the running point of highest simulated pressure ratio at 3890 rpm/$K^{0.5}$ [19]. As this procedure is time consuming and a changed geometry for each speed line is not desired for the analysis the VGT has been maintained at the same position. Although this might cause small differences between experimental and CFD model VGT opening, the qualitative behavior of efficiency and mass flow curve have been well reproduced by CFD over the entire range of the 3 highest speeds. At the lowest speed, efficiencies estimated by CFD are within the measurement errors, which are naturally high at points of low power output and small expansion ratios.

3 Tip Leakage Flow Analysis

The comparison of CFD results with different tip gap heights shows that this geometry change can influence significantly the turbine efficiency and rather less reduced mass flow like it has also been stated in [11]. From the wide range data it can further be seen that the difference in efficiency diminishes towards very low pressure ratios/high BSRs with varying tip gap height. According to [14] the tip leakage flow is mainly dominated by pressure driven leakage flow (positive direction in relative frame according to Fig. 5) and friction driven flow through the tip gap (negative direction in relative frame according to Fig. 5). The CFD results are consistent with the observation that tip leakage mass flow in

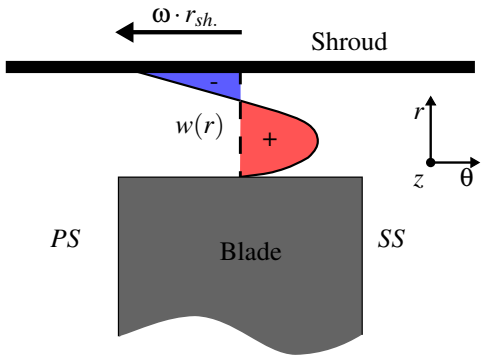

Figure 5: Definition of positive and negative tip flow.

positive direction decreases due to lower blade loading. Nevertheless, the relative part of negative tip mass flow $\frac{\dot{m}_{\text{tip},-}}{\dot{m}_{\text{turb.}}}$ increases going towards operating conditions with low loads [18]. Thus, increasing parts of the mass flow are not used for enthalpy extraction.

In Fig. 6 and Fig. 7 profiles of specific mass flow in blade normal direction through the tip gap are shown for two running points (marked blue in Fig. 3 (b) at 3890 rpm/K$^{0.5}$). The first shows a running point close to design condition with low incidence. The later shows the flow at off-design condition and a high mean inflow incidence β of −51°. Since, the flow profile close to design conditions looks rather undisturbed the diminishing influence of wall friction can be observed towards higher chord length. The higher radius in the inducer of the radial turbine causes faster relative shroud velocity. This generates a stronger fluid dragging effect in the inducer. Hence, the maximum specific mass flow increases continuously up to a chord length of around 0.7. Looking at

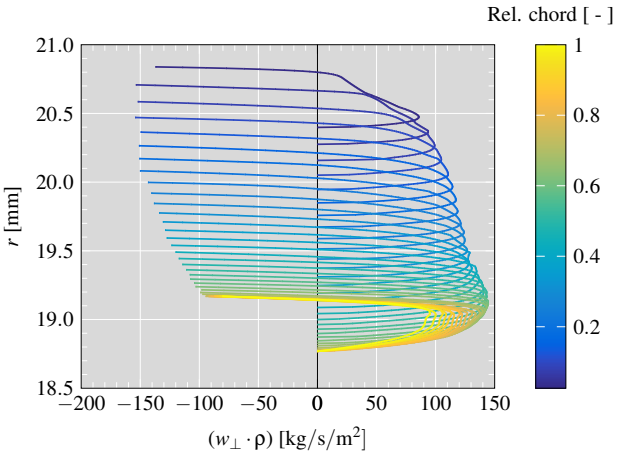

Figure 6: Tip leakage flow profiles of low negative incidence inlet flow over the tip gap at 3890 rpm/K$^{0.5}$ and a $\pi_{\text{turb.}}$ of 1.37

the profiles in Fig. 7 a clear influence of the incidence flow can be seen. Maximums of positive specific mass flow seem to decrease by the contrariwise inflow momentum. On the one hand side, losses generated by positive tip flow might be reduced. On the other hand side, new losses are introduced by entropy increasing negative tip flow. Due to the pulsat-

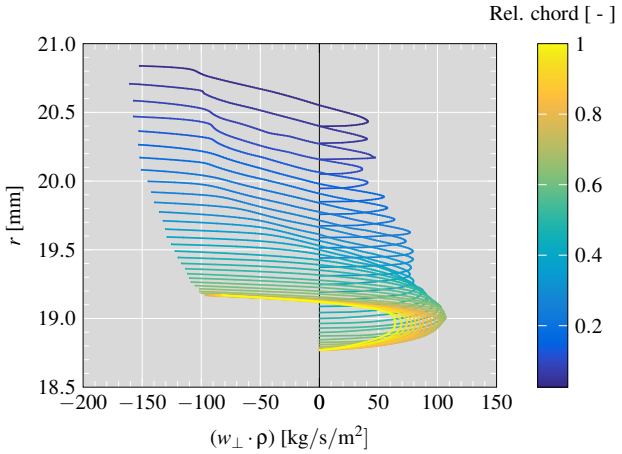

Figure 7: Tip leakage flow profiles of high negative incidence inlet flow over the tip gap at 3890 rpm/K$^{0.5}$ and a $\pi_{\text{turb.}}$ of 1.29

ing flow in a turbocharger turbine, the turbine can operate in zones of extremely high incidences. This and the complexity of the tip leakage flow at design and off-design conditions highlights the importance of understanding the dynamic of this loss generating process.

Equation 2 for the tip loss coefficient Y, that has been proposed in [17], is widely used in the literature to correlate the relative tip velocity w with produced losses.

$$Y = \frac{l_{\text{tip}} \cdot \int 0.5 \cdot \rho \cdot w_{\perp,\text{tip}} \cdot w_{\perp,\text{tip}}^2 \, \mathrm{d}r}{\dot{m}_{\text{turb.}} \cdot \Delta h_0} \tag{2}$$

Dambach et. al [14] showed experimentally that the ratio of chordwise positive and negative momentum behaves qualitatively as the specific tip loss coefficient over the chord length. Thus, it has been recommended to formulate the momentum ratio of both leakage flows for characterizing tip flow as:

$$R = \frac{M_{\text{tip},+}}{M_{\text{tip},-}} = \frac{\Delta p_{(\text{PS,SS})}}{\rho \omega^2 r_{\text{sh.}}^2 \cos\gamma^2}. \tag{3}$$

Here, the only needed fluid number is the surface pressure difference between SS and PS close to the wall, which makes this number easy to use.

In Fig. 8 pressure profiles for the with red circles marked running points of Fig. 3 (d) have been presented over the chord length. While the pressure profile changes rather less when the gap height is reduced, blade loading at the tip cannot be conserved in the same quality when the tip gap is 50 % increased.

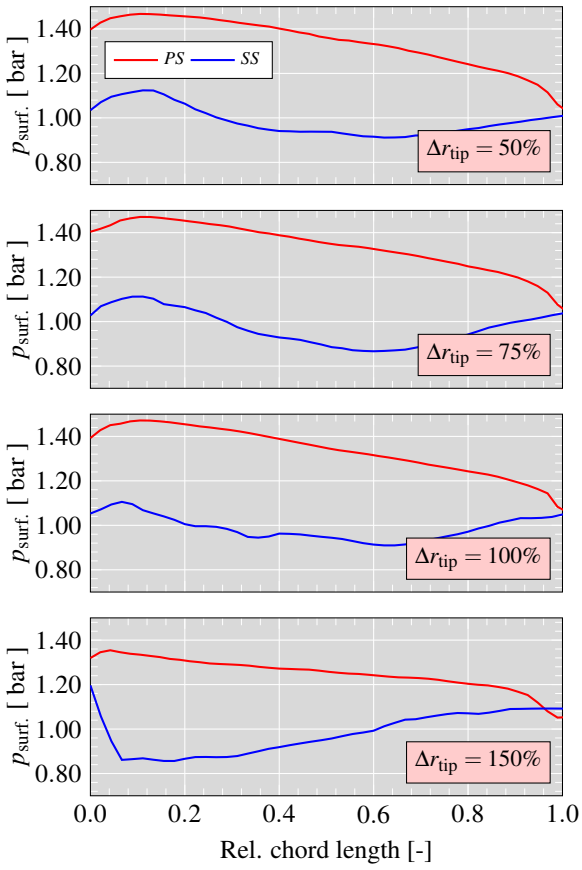

Figure 8: Surface pressure profiles at 95 % span for four different tip gap geometries at 6715 rpm/K$^{0.5}$ and 60 % VGT opening (red circle in Fig. 3 (d))

Further, the simulated specific momentum trough the tip gap over a line at constant chord length has been processed from the CFD data according to Eqn. 4 and Eqn. 5 in positive and negative direction.

$$M_{\text{tip,spec.,+}} = \int_{r_{\text{tip}}}^{r_{(w_{\perp,\text{tip}}=0)}} \rho \cdot w_{\perp,\text{tip}} \cdot w_{\perp,\text{tip}} \, \mathrm{d}r \,. \tag{4}$$

$$M_{\text{tip,spec.,-}} = \int_{r_{(w_{\perp,\text{tip}}=0)}}^{r_{\text{sh.}}} \rho \cdot w_{\perp,\text{tip}} \cdot w_{\perp,\text{tip}} \, \mathrm{d}r \,, \tag{5}$$

The simulated momentum ratio R_{CFD} has following been calculated by:

$$R_{\text{CFD}} = \frac{M_{\text{tip,spec.,+}}}{M_{\text{tip,spec.,-}}} \,. \tag{6}$$

In Fig. 9 the ratio R has been plotted over the chord length in comparison with R_{CFD} for the running points with different tip gap configurations in red circles from Fig. 3 (d) (with different y-axis for R_{CFD} and R). It can be seen that

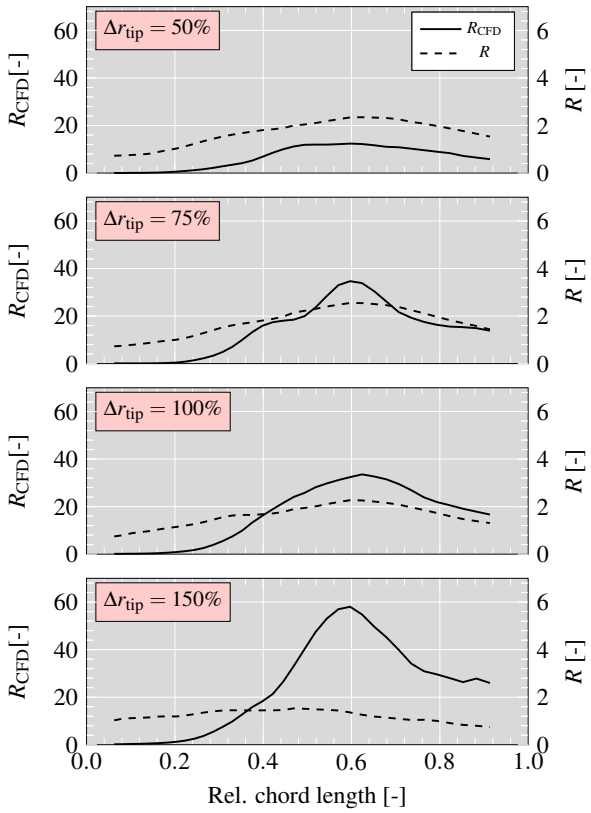

Figure 9: Momentum ratios R (Eqn. 3), R_{CFD} (Eqn. 6) for four different tip gap heights at 6715 rpm/K$^{0.5}$ and 60 % VGT opening (red circles in Fig. 3 (d))

R misses the simulated momentum ratio R_{CFD} by one magnitude. However, the ratio R gives a rather good qualitative prediction of the maximum location of the simulated mass flow ratio over the chord length for the first two tip gap setups of 50 % and 100 %. Since the pressure profile is the only input data from the fluid and no detailed tip geometry data is required for calculating R, it also fails to predict the momentum ratio growth with increasing tip gap height. With the tip gap configuration of $\Delta r_{\text{tip}} = 150\%$ the momentum ratio experiences an unexpected rise at around 0.6 chord length. At such a relatively high tip gap height the flow seems to be less dominated by the pressure gradient and high values of R_{CFD} are reached by passing flow momentum from the blade passage that cannot be guided by the turbine blades. Furthermore, it can be seen in Fig. 9 that all R_{CFD} profiles experience a sudden drop towards the turbine inlet. This drop has four main sources:

1. Higher shroud friction influence due to angle between blade and rotational axis (blade surface angle γ) in the inducer [14].
2. Slightly higher shroud radius and thus, increased shroud friction [14].
3. High impact of inflow momentum due to negative incidence.
4. Swapped pressure gradient due high negative incidence and flow separation at the leading edge.

The incidence flow through the tip gap causes an entropy increase and can be considered as additional loss. Furthermore, the determination of related mass flow and momentum is rather challenging since the aforementioned effects are mixed.

4 Method for Tip Leakage Flow Characterization

For one dimensional modeling and for design purposes it can be important to distinguish friction and pressure driven effects in the tip leakage flow from other effects as incidence flow or blow by and to be able to estimate the quantity of this loss generating flow phenomena dependent on geometrical details. Since the mentioned momentum ratio correlates qualitatively well along the chord length with estimated loss productions but misses to predict the qualitative change in momentum ratio when geometry is changed, the correlation of both momentum flows has newly been derived in the following.

4.1 Novel Momentum Ratio

Starting from the Navier Stokes equation in a cylindrical rotational reference frame Eqn. 7 has been simplified under the assumptions: $\frac{\partial}{\partial t}, \frac{\partial}{\partial \theta}, \frac{\partial}{\partial z}, w_\mathrm{r} = 0$.

$$\begin{aligned}
&\rho\left(\frac{\partial w_\theta}{\partial t} + w_\mathrm{r}\frac{\partial w_\theta}{\partial r} + \frac{w_\theta}{r}\frac{\partial w_\theta}{\partial \theta} + \frac{w_\mathrm{r} w_\theta}{r} + w_\mathrm{z}\frac{\partial w_\theta}{\partial z}\right) \\
&= -\frac{1}{r}\frac{\partial p}{\partial \theta} + \rho g_\theta - 2\rho\omega w_\mathrm{r} + \\
&+\mu\left[\frac{1}{r}\frac{\partial}{\partial r}\left(r\frac{\partial w_\theta}{\partial r}\right) - \frac{w_\theta}{r^2} + \frac{1}{r^2}\frac{\partial^2 w_\theta}{\partial \theta^2} + \frac{2}{r^2}\frac{\partial w_\mathrm{r}}{\partial \theta} + \frac{\partial^2 w_\theta}{\partial z^2}\right]
\end{aligned} \tag{7}$$

Based on this assumption and a calculation applying various substitutions, solving the resulting inhomogeneous differential equation with non-constant coefficients and integrating over the tip gap led to Eqn. 8 and Eqn. 9. The derivation has been done in [18].

$$\begin{aligned}
\bar{w}_{\mathrm{tip},\theta,+} = &\left\{\left[\frac{r_\mathrm{tip}^2 - r_\mathrm{sh.}^2}{4} + \frac{r_\mathrm{sh.}^2}{2}\cdot\ln\left(\frac{r_\mathrm{sh.}}{r_\mathrm{tip}}\right)\right] - \right. \\
&\left. - \frac{\left[\frac{r_\mathrm{sh.}^2 - r_\mathrm{tip}^2}{2\cdot r_\mathrm{tip}^2} + \ln\left(\frac{r_\mathrm{tip}}{r_\mathrm{sh.}}\right)\right]}{\left(\frac{r_\mathrm{sh.}}{r_\mathrm{tip}^2} - \frac{1}{r_\mathrm{sh.}}\right)}\cdot\left[r_\mathrm{sh.}\ln\left(\frac{r_\mathrm{sh.}}{r_\mathrm{tip}}\right)\right]\right\}\cdot \\
&\cdot\frac{1}{2}\frac{1}{\mu}\frac{\Delta p_\mathrm{(PS,SS)}}{\Delta\theta\Delta r_\mathrm{tip}}
\end{aligned} \tag{8}$$

$$\bar{w}_{\mathrm{tip},\theta,-} = \frac{\left[\frac{r_\mathrm{sh.}^2 - r_\mathrm{tip}^2}{2\cdot r_\mathrm{tip}^2} + \ln\left(\frac{r_\mathrm{tip}}{r_\mathrm{sh.}}\right)\right]}{\left(\frac{r_\mathrm{sh.}}{r_\mathrm{tip}^2} - \frac{1}{r_\mathrm{sh.}}\right)}\cdot\frac{\omega\cdot r_\mathrm{sh.}\cdot\cos\gamma}{\Delta r_\mathrm{tip}} \tag{9}$$

Here, the leading effects of wall friction and pressure difference between SS and PS have already been separated to model the mean relative velocity of the negative and positive tip leakage flow. Furthermore, the geometrical terms (including $r_\mathrm{sh.}$ and r_tip) have been concentrated into one factor. Next, the momentum ratio has been defined as:

$$R_\mathrm{NS} = \frac{\rho_+}{\rho_-}\cdot\frac{\bar{w}_{\mathrm{tip},\theta,+}^2}{\bar{w}_{\mathrm{tip},\theta,-}^2} \tag{10}$$

Substituting Eqn. 8 and Eqn. 9 in Eqn. 10 the novel momentum ratio can be described as:

$$\begin{aligned}
R_\mathrm{NS} = \frac{\rho_+}{\rho_-}\cdot\left\{\frac{\left(\frac{r_\mathrm{sh.}}{r_\mathrm{tip}^2} - \frac{1}{r_\mathrm{sh.}}\right)\left[\frac{r_\mathrm{tip}^2 - r_\mathrm{sh.}^2}{4} + \frac{r_\mathrm{sh.}^2}{2}\cdot\ln\left(\frac{r_\mathrm{sh.}}{r_\mathrm{tip}}\right)\right]}{\left[\frac{r_\mathrm{sh.}^2 - r_\mathrm{tip}^2}{2\cdot r_\mathrm{tip}^2} + \ln\left(\frac{r_\mathrm{tip}}{r_\mathrm{sh.}}\right)\right] r_\mathrm{sh.}} - \right. \\
\left. - \ln\left(\frac{r_\mathrm{sh.}}{r_\mathrm{tip}}\right)\right\}^2\left\{\frac{\frac{1}{2}\frac{1}{\mu}\frac{\Delta p_\mathrm{(PS,SS)}}{\Delta\theta}}{\omega\cos\gamma}\right\}^2
\end{aligned} \tag{11}$$

It can be seen that only the viscosity and the pressure on SS and PS are required from the flow to calculate the ratio. The viscosity has been assumed to be rather constant here. Simulation results have shown that the density ratio is close to 1. For the purpose of simplicity and for later analysis the following nomenclature has been chosen for the purely geometry dependent factor and the "fluid" factor:

$$R_\mathrm{geo.} = \left\{\frac{\left(\frac{r_\mathrm{sh.}}{r_\mathrm{tip}^2} - \frac{1}{r_\mathrm{sh.}}\right)\left[\frac{r_\mathrm{tip}^2 - r_\mathrm{sh.}^2}{4} + \frac{r_\mathrm{sh.}^2}{2}\cdot\ln\left(\frac{r_\mathrm{sh.}}{r_\mathrm{tip}}\right)\right]}{\left[\frac{r_\mathrm{sh.}^2 - r_\mathrm{tip}^2}{2\cdot r_\mathrm{tip}^2} + \ln\left(\frac{r_\mathrm{tip}}{r_\mathrm{sh.}}\right)\right] r_\mathrm{sh.}} - \ln\left(\frac{r_\mathrm{sh.}}{r_\mathrm{tip}}\right)\right\}^2 \tag{12}$$

$$R_\mathrm{fl.} = \left\{\frac{\frac{1}{2}\frac{1}{\mu}\frac{\Delta p_\mathrm{(PS,SS)}}{\Delta\theta}}{\omega\cos\gamma}\right\}^2 \tag{13}$$

$$R_\mathrm{NS} = \frac{\rho_+}{\rho_-}\cdot R_\mathrm{geom.}\cdot R_\mathrm{fl.} \tag{14}$$

It is worth highlighting that $R_\mathrm{fl.}$ would result in extremely high values, if $\Delta\theta$ would be defined by the small blade thickness. This might be the case because $\frac{\partial}{\partial\theta} = 0$ has been assumed deriving the final equations. This is an assumption for developed flow, which is apparently not the

case after the short distance of a tip gap. However, this assumption overcomes estimating a flow profile at tip gap inlet to obtain a gap flow profile at the outlet and makes the solution of the Navier Stokes equation much easier, while maintaining the main trends. Thus, $\Delta\theta$ must be understood as an effective flow length $\Delta\theta_{\text{eff.}}$ and has been analyzed in more detail.

4.2 Effective Flow Length

The momentum ratio obtained from the CFD simulations has been used to calculate the effective flow length:

$$\Delta\theta_{\text{eff.}} = \sqrt{\frac{\rho_+}{\rho_-} \cdot \frac{R_{\text{geom.}}}{R_{\text{CFD}}}} \cdot \frac{\frac{1}{2}\frac{1}{\mu}\Delta p_{(\text{PS,SS})}}{\omega \cos\gamma} \tag{15}$$

$\Delta\theta_{\text{eff.}}$ is expected to behave as the discharge coefficient appearing in publications about flow characterization of flow through an orifice [25] and thus, can be characterized by means of the Reynolds numbers of both flow directions:

$$Re_+ = \frac{\rho_+ \cdot \bar{w}_{\text{tip},\theta,+} \cdot \Delta r_{\text{tip}}}{\mu}, \tag{16}$$

$$Re_- = \frac{\rho_- \cdot \omega \cdot r_{\text{sh.}} \cdot \Delta r_{\text{tip}} \cdot \cos\gamma}{\mu} \tag{17}$$

It has been found out that plotting $\Delta\theta_{\text{eff.}}$ over the ratio $\frac{Re_-}{Re_+^{1/6}}$ gives a clear trend for all simulated points as Fig. 10 shows.

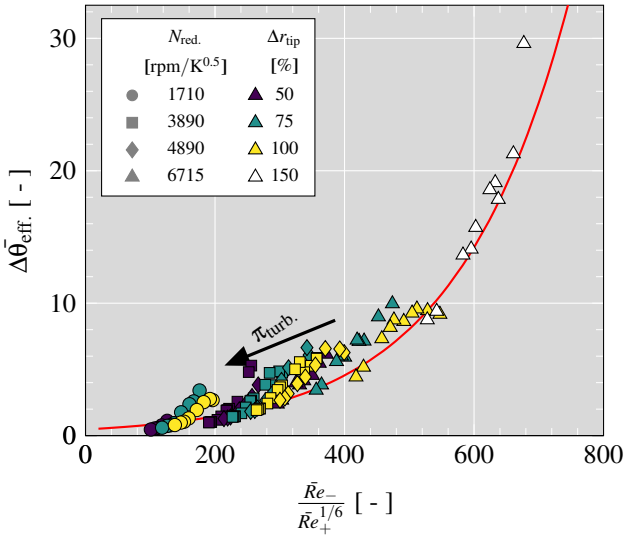

Figure 10: Fitting of $\Delta\bar{\theta}_{\text{eff.}}$ values

Here, average values from 0 % to 100 % chord length have been used to reduce complexity. Towards off-design condition the aforementioned influence of the incidence flow momentum on the momentum ratio causes higher values of the mean effective inflow length and explains the deviation from the overall trend for those points. The global trend is independent of the tip gap height Δr_{tip}, the rotational speed $N_{\text{red.}}$ and of the overall turbine pressure ratio $\pi_{\text{turb.}}$.

Since friction and pressure driven effects have been decoupled to obtain the ratio R_{NS}, the relation in Fig. 10 represents the coupling of both flows due to fluid friction. $\Delta\theta_{\text{eff.}}$ is increasing with rising rotational speed (increase of friction layer and reduction of effective area for pressure driven flow) and is decreasing when $\pi_{\text{turb.}}$ (and thus $\Delta p_{(\text{PS,SS})}$) is increasing. Apparently, the relation of $\Delta\theta_{\text{eff.}}$ is dependent on itself, when Eqn. 16 is calculated with the proposed formula in Eqn. 8:

$$\Delta\theta_{\text{eff.}} = f\left(\frac{Re_-}{f(\Delta\theta_{\text{eff.}})}\right). \tag{18}$$

The data can directly be fitted with an exponential equation as it can be seen in 10. However, this would only allow an iterative solution, what causes difficulties in the further analysis and conclusions. Since an analytical solution is aimed $\Delta\theta_{\text{eff.}}$ has been fitted with a simple parabolic function:

$$\Delta\theta_{\text{eff.}} = a \cdot \left(\frac{Re_-}{Re_+^{1/6}}\right)^b. \tag{19}$$

Following, the analytical solution of R_{NS} can be obtained by substituting Eqn. 19, Eqn. 16, Eqn. 17 in Eqn. 11 and considering $\Delta\theta$ as $\Delta\theta_{\text{eff.}}$:

$$R_{\text{NS}} = a^{\frac{12}{6-b}} \cdot \frac{\rho_+}{\rho_-} \cdot R_{\text{fl.,eff.}} \cdot R_{\text{mix,eff.}} \cdot R_{\text{geom.,eff.}}$$

with :

$$R_{\text{fl.,eff.}} = \left(\frac{1}{2}\frac{1}{\mu}\frac{\Delta p_{(\text{PS,SS})}}{\omega\cos\gamma}\right)^{\frac{12}{6-b}},$$

$$R_{\text{mix,eff.}} = \left(\frac{\rho_+}{\rho_-^6}\right)^{\frac{2\cdot b}{6-b}} \cdot \left\{\frac{\mu^5}{(\cos\gamma\cdot\omega)^5}\right\}^{\frac{2\cdot b}{6-b}} \cdot \left(\frac{1}{\Delta r_{\text{tip}}^5 \cdot r_{\text{sh.}}^5}\right)^{\frac{2\cdot b}{6-b}},$$

$$R_{\text{geom.,eff}} = R_{\text{geom.}}^{\frac{6}{6-b}} \cdot \left\{\frac{\left[\frac{r_{\text{sh.}}^2 - r_{\text{tip}}^2}{2\cdot r_{\text{tip}}^2} + \ln\left(\frac{r_{\text{tip}}}{r_{\text{sh.}}}\right)\right]}{\left(\frac{r_{\text{sh.}}}{r_{\text{tip}}^2} - \frac{1}{r_{\text{sh.}}}\right)\Delta r_{\text{tip}}}\right\}^{\frac{2\cdot b}{6-b}}. \tag{20}$$

It can be seen that the factor $R_{\text{geom.}}$ has been extended and changes its exponent as well as $R_{\text{fl.}}$. Additionally, a third

non-dimensional factor arises. This factor consists of geometry data and fluid information to model and is needed (together with aforementioned modifications of the equation) to model the interaction between wall friction flow and pressure driven flow.

5 Model Results & Discussion

5.1 Model Fitting

By means of a nonlinear fitting the MATLAB coded model has been fitted towards the chordwise R_{CFD} values of all simulated points including all tip gap configurations. The fitting coefficients have been obtained as $a = 1250$ and $b = 1.23$. Mean values of each tip gap and running point of R_{CFD} have been reproduced in good quality for the most analyzed points as it can be seen in Fig. 11.

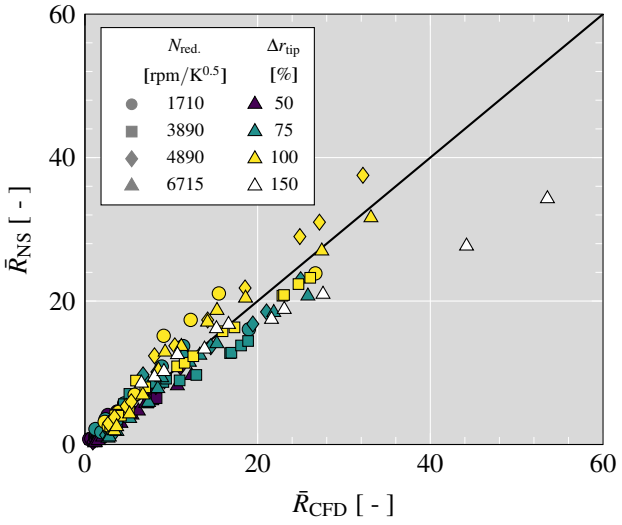

Figure 11: Mean values for momentum ratio R_{NS} with simple exponential function (Eqn. 19)

The two points marked in 11 are those of highest mass flow $\dot{m}_{red.,turb.}$ and biggest tip gap configuration. In these conditions the proposed model underestimates the mean momentum ratio $\bar{R}_{NS}$. This could be caused by operating close to choke condition and thus increasing simulated momentum flow through the tip gap.

Since the momentum through the tip gap can be related with the tip clearance losses and good fitting quality has been achieved for mean values of R_{NS}, the presented correlation might help to further reduce the number of fitting coefficients in one dimensional tip leakage models like the one described in [18]. Furthermore, the dependence on the geometry as blade angle γ, blade radius r_{tip}, and tip gap height Δr_{tip} allows to increase model sensibility for the analysis and prediction of the tip leakage flow and losses for a bigger range of unmeasured geometries.

Apart from the capability to obtain good estimations for the mean value of R_{NS}, the fitted model can be applied to do further qualitative analysis. In Fig. 12 it can be seen that the ratio R_{NS} is well predicted over the chord length for the 50 %, 75 %, and the 100 % tip gap configuration. R_{NS} is able to catch the high momentum ratio reduction close to 0, at lower relative chord lengths, that R was not able to predict. As mentioned before, the characteristic tip leakage flow with the biggest tip gap is affected by unguided passage flow momentum. This effect cannot be predicted by the model, since this is based the blade loading and friction driven flow. Although this represents a limitation of the chordwise modeling, such values of the tip gap heights are technically less relevant.

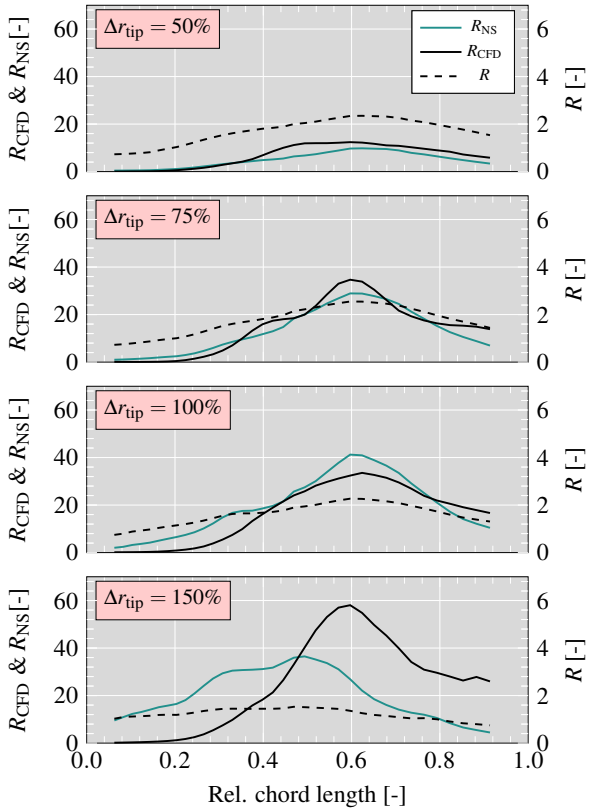

Figure 12: Momentum ratios R (Eqn. 3), R_{CFD} (Eqn. 6), and R_{NS} (Eqn. 20) for four different tip gap heights at 6715 rpm/K$^{0.5}$ and 60 % VGT opening (red circles in Fig. 3 (d))

Concluding, the modeled momentum ratio R_{NS} is able to reproduce the following trend: there are higher parts of pressure driven momentum flows through the tip gap, when the tip gap becomes bigger, even when the blade loading changes only slightly or decreases.

5.2 Momentum Ratio Analysis

While a non-dimensional analysis of the factors $R_{fl.,eff.}$ require further assumptions of the blade loading or rotational speed, the newly gained factors $R_{geom.,eff.}$ of Eqn. 20 can be analyzed only dependent on geometry variations. Since

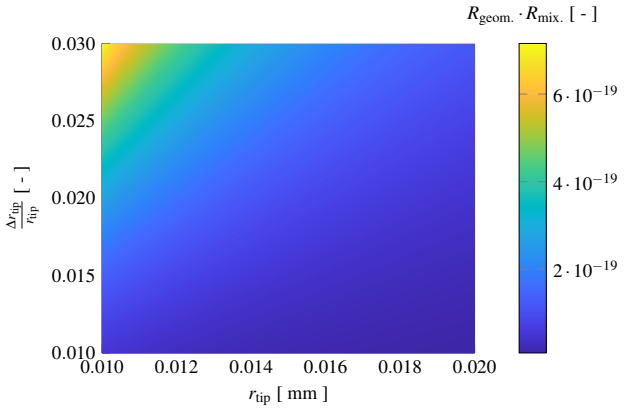

Figure 13: Geometry changes vs. geometrical factor $R_{geom.,eff.}$ times mixed factor $R_{mix,eff.}$

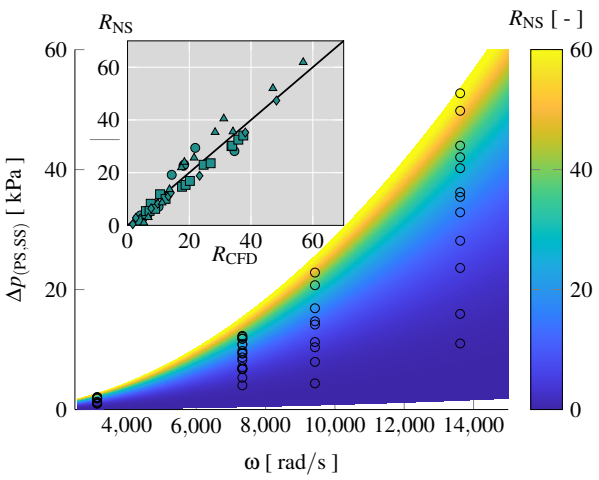

Figure 14: Model results and validation for the points of highest $\Delta p_{(PS,SS)}$ per running point. Color: radial velocity and local blade loading vs. momentum ratio R_{NS}; Dots: simulated rotational velocity and maximum local blade loading in the exducer for each running point; Small: Momentum ratio R_{NS} vs. momentum ratio R_{CFD} at highest local blade loading close to the tip.

the mixed ratio $R_{mix,eff.}$ has further variables as density ratio, blade angle correlations and radial velocity, assumptions and simplifications have had to be made for continuing the analysis. While the impact of the density and the blade angle have been neglected (= 1), a constant angle velocity of 14 347 rad/s ($U_{in} = 300 m/s$) has been assumed. For analyzing the overall impact of geometry changes on the momentum ratio, the newly gained ratio $R_{mix,eff.}$ with the aforementioned assumptions has been multiplied with $R_{geom.,eff.}$ as it can be seen in Fig. 13. The factor $R_{geom.,eff.} \cdot R_{mix,eff.}$ increases exponentially with decreasing tip radius r_{tip} and increasing $\frac{\Delta r_{tip}}{r_{tip}}$. This confirms independent from the factor $R_{fl.,eff.}$, which includes local blade loading and rotational speed, a tendency to higher positive leakage momentum and related losses at lower radius. Thus, front loaded blade designs are in favor of a minimization of tip leakage losses.

Finally, Fig. 14 shows the entire ratio of Eqn. 20 in dependence of the variables ω and $\Delta p_{(PS,SS)}$, which are defining $R_{fl.}$. As geometry input for r_{tip}, $r_{sh.}$, and $cos\gamma$ constant values have been set. Here, the geometry of the chord length with highest blade loading that has been found for the most CFD solutions has been taken (with Δr_{tip} = 100 %). The highest blade loading occurs mostly close to 60 % chord length, in the exducer section. Also, the highest found blade loading for each simulated running point has been shown against the radial velocity to highlight the simulated operating range and relevant values for R_{NS}. To evaluate the validity of the presented model results, a comparison of the momentum ratios $R_{CFD,\Delta pmax}$ and $R_{NS,\Delta pmax}$ at described location has been shown in Fig. 14. The given trends are well reproduced by the found correlation.

In Fig. 14 it can be seen that each simulated speed covers a similar range of R_{NS} from low values (1.7-5.3) up to values around 40 and higher. While the momentum ratio is changing rather less at off-design conditions with lower blade loading, a small increase in the local blade loading $\Delta p_{(PS,SS)}$ can cause a significant increase of the momentum ratio and thus, of the tip leakage losses when operating at high efficiencies and close to design condition. This inherent sensitivity of the tip leakage momentum ratio on $\Delta p_{(PS,SS)}$ highlights, why the model results at nearly design condition in Fig. 12 can be considered as relatively good.

5.3 Tip Leakage Velocity Fitting

As in Eqn. 2 many tip leakage loss correlations are based on the positive tip leakage velocity. By using Eqn. 8 and correlating the effective inflow length with:

$$\Delta\theta_{eff.} = c \cdot (Re_{-})^{b}. \tag{21}$$

good fittings have been achieved with CFD data for modeled $\bar{w}_{tip,\theta,+}$ as it can be seen in Fig. 15. Here, $\Delta\theta_{eff.}$ does only depend on the the negative Reynolds number as it has been defined in Eqn. 17 and the same exponent that has been found for the momentum ratio can be applied. This way only one additional coefficient is necessary. The factor c has been fitted with 2332.

5.4 Incidence Flow Analysis

As highlighted before, incidence flow has significant influence on the momentum ratio in the rotor inlet and contributes to the tip leakage loss itself. Hence, the evaluation of this mixed flow effect can be of high importance. Taking advantage of the already found correlation for the momentum ratio and positive leakage velocity, the mean negative velocity and momentum driven by shroud friction can be found by:

$$\bar{w}_{tip,\theta,-,NS} = \sqrt{\frac{\rho_{+}}{\rho_{-}} \frac{\bar{w}^{2}_{tip,\theta,+,NS}}{R_{NS}}} \tag{22}$$

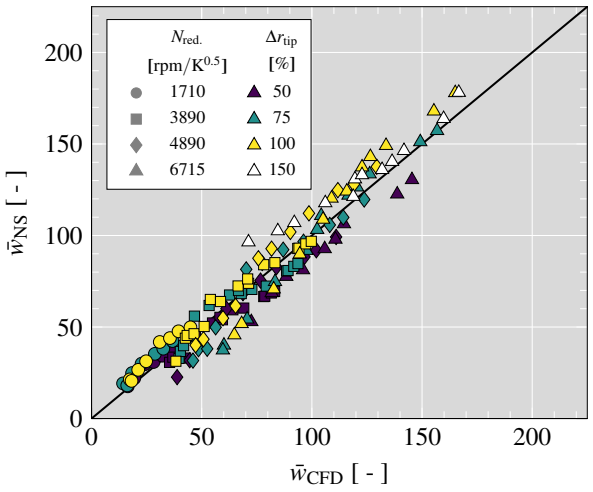

Figure 15: Fitting of $\bar{w}_{\mathrm{tip},\theta,+}$: model vs. CFD data

$$\bar{M}_{\mathrm{tip},-,\mathrm{NS}} = \rho \bar{w}^2_{\mathrm{tip},\theta,-,\mathrm{NS}} \tag{23}$$

In Fig. 16 the chordwise integral of this momentum has been compared with the same value from the CFD results for the entire speedline of 3890 rpm/K$^{0.5}$, since this speed has running points from very low incidence to high negative incidence. Calculating the deviation between both shows clearly values close to zero when the inflow incidence is low and rising values towards higher negative incidence. This highlights again the validity of the before derived correlations as well as the capability to use those for further analysis of the incidence flow. Finally, the filtered incidence flow momentum can be fitted in good quality with $9 \cdot (1 - \cos(i))$ as it has been demonstrated in Fig. 16.

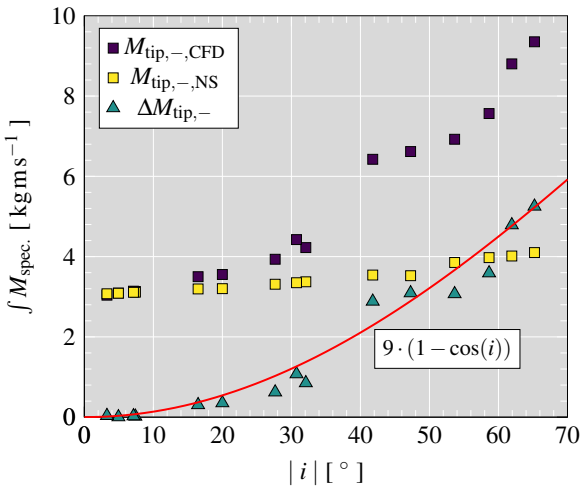

Figure 16: Chordwise integral of negative momentum and difference between CFD and model at 3890 rpm/K$^{0.5}$ and 100 % tip gap opening

6 Conclusions

The main conclusions of the work are highlighted as follows:

1. Steady state simulations at four different reduced speeds with three different tip gap variations (four tip gap variations at highest speed) have been executed in a wide range of operating conditions.
2. Incidence flow has been identified to influence the tip leakage specific mass flow and momentum. While it reduces the pressure induced specific mass flow in the tip gap at low chord length, the incidence inflow leads to an increase of inverse directed specific mass flow, which causes a further entropy rise.
3. The ratio of friction and pressure ratio driven momentum has been analyzed and it has been stated that available correlations are not capable of doing quantitative conclusions of tip leakage flow over the chord length and neither qualitative conclusions of geometry changes.
4. A new correlation to calculate the momentum ratio based on the Navier Stokes Equation has been derived. The equation inherent flow length, here interpreted as effective flow length, has been fitted dependent on the ratio of Reynolds numbers build for friction driven and pressure driven flow $\frac{Re_-}{Re_+^{1/6}}$ for all analyzed running conditions at design and off-design, from low to high rotational speed, and for varied geometry.
5. It has been demonstrated that the tip leakage flow reacts sensitive on small changes in the tip close blade loading when operating close to design conditions. With slightly higher pressure between SS and PS the momentum ratio and related losses can increase significantly.
6. One additional correlation has been found to fit the pressure driven velocity, which allows to calculate the impact of friction momentum and to analyze the impact of the incidence flow momentum.
7. Found correlations can directly been used in efficiency extrapolation models that rely on tip leakage velocities or momentums. As demonstrated the correlations can further been used to analyze mixed flow phenomena in the tip leakage flow. Also, found trends can be of interest for turbocharger turbine designer.

7 Acknowledgments

The work has been partially supported by FEDER and the Spanish Ministry of Economy and Competitiveness through grant number TRA2016-79185-R.

Authors want to thank intern Niki Wilms for his valuable work.

References

[1] European Parliament, Council of the European Union, 2007. “Regulation (EC) No 715/2007 of the European Parliament and of the Council of 20 June 2007 on type approval of motor vehicles with respect to emissions from light passenger and commercial vehicles (Euro 5

and Euro 6) and on access to vehicle repair and maintenance information (Text with EEA relevance) ". *Official Journal of the European Union,* **50**, June, pp. 1–16.

[2] Serrano, J. R., Olmeda, P., Tiseira, A., García-Cuevas, L. M., and Lefebvre, A., 2013. "Theoretical and experimental study of mechanical losses in automotive turbochargers". *Energy,* **55**, pp. 888–898.

[3] Galindo, J., Fajardo, P., Navarro, R., and García-Cuevas, L. M., 2013. "Characterization of a radial turbocharger turbine in pulsating flow by means of CFD and its application to engine modeling". *Applied Energy,* **103**(0), pp. 116 – 127.

[4] Romagnoli, A., and Martínez-Botas, R., 2011. "Performance prediction of a nozzled and nozzleless mixed-flow turbine in steady conditions". *International Journal of Mechanical Sciences,* **2011**(53), pp. 557–574.

[5] Salameh, G., Chesse, P., and Chalet, D., 2016. "Different measurement techniques for wider small radial performance maps". *Experimental Techniques,* **40**(6), 12, pp. 1511–1525.

[6] Serrano, J. R., Tiseira, A., García-Cuevas, L. M., Inhestern, L. B., and Tartoussi, H., 2017. "Radial turbine performance measurement under extreme off-design conditions". *Energy,* **125**, pp. 72 – 84.

[7] Serrano, J. R., García-Cuevas, L. M., Inhestern, L. B., Mai, H., Rinaldi, A., and Miguel-Sanchez, A., 2017. "Methodology to evaluate turbocharger turbine performance at high blade to jet speed ratio under quasi adiabatic conditions". In ASME. Turbo Expo: Power for Land, Sea, and Air, Volume 8: Microturbines, Turbochargers and Small Turbomachines; Steam Turbines ():V008T26A004., American Society of Mechanical Engineers.

[8] Romagnoli, A., and Martinez-Botas, R., 2011. "Performance prediction of a nozzled and nozzleless mixed-flow turbine in steady conditions". *International Journal of Mechanical Sciences,* **53**(8), pp. 557 – 574.

[9] Serrano, J. R., Arnau, F. J., García-Cuevas, L. M., Dombrovsky, A., and Tartousi, H., 2016. "Development and validation of a radial turbine efficiency model at extreme off-design conditions". *Energy Conversion and Management*.

[10] Baines, N., 1998. "A meanline prediction method for radial turbine efficiency". In IMECHE conference transactions, Vol. 11, Mechanical Engineering Publications, pp. 45–56.

[11] Kammeyer, J., Natkaniec, C., and Seume, J. R., 2010. "Tip leakage in small radial turbines: Optimum tip-gap and efficiency loss correlations". In ASME Turbo Expo 2010: Power for Land, Sea, and Air, American Society of Mechanical Engineers, pp. 391–401.

[12] Kammeyer, J., Natkaniec, C., and Seume, J. R., 2010. "Influence of tip-gap losses on the stage efficiency of downsizing turbocharger turbines". In 9th International Conference on Turbochargers and Turbocharging,19-20 May, London.

[13] Baines, N., 2006. "Radial turbine design". In Axial and Radial Turbines, Concepts NREC.

[14] Dambach, R., Hodson, H., and Huntsman, I., 1998. "An experimental study of tip clearance flow in a radial inflow turbine". In ASME. Turbo Expo: Power for Land, Sea, and Air, Volume 1: Turbomachinery ():V001T01A110., American Society of Mechanical Engineers.

[15] Dambach, R., and Hodson, H., 2001. "Tip leakage flow in a radial inflow turbine with varying gap height". *Journal of Propulsion and Power,* **17**(3), pp. 644–650.

[16] Dambach, R., Hodson, H., and Huntsman, I., 2002. "Tip-leakage flow: a comparison between axial and radial turbines". *Micro-Turbine Generators*, p. 97.

[17] Yaras, M., and Sjolander, S., 1992. "Prediction of tip-leakage losses in axial turbines". *ASME J. Turbomach,* **114**(1), pp. 204–210.

[18] Serrano, J. R., Navarro, R., Garca-Cuevas, L. M., and Inhestern, L. B., 2018. "Turbocharger turbine rotor tip leakage loss and mass flow model valid up to extreme off-design conditions with high blade to jet speed ratio". *Energy,* **147**, pp. 1299 – 1310.

[19] Serrano, J. R., Gil, A., Navarro, R., and Inhestern, L. B., 2017. "Extremely low mass flow at high blade to jet speed ratio in variable geometry radial turbines and its influence on the flow pattern: A CFD analysis". In ASME. Turbo Expo: Power for Land, Sea, and Air, Volume 8: Microturbines, Turbochargers and Small Turbomachines; Steam Turbines ():V008T26A005., American Society of Mechanical Engineers.

[20] Menter, F. R., 1994. "Two-equation eddy-viscosity turbulence models for engineering applications". *AIAA journal,* **32**(8), pp. 1598–1605.

[21] Menter, F. R., Langtry, R., and Hansen, T., 2004. "CFD simulation of turbomachinery flows verification, validation and modeling". In European Congress on Computational Methods in Applied Sciences and Engineering, ECCOMAS.

[22] Simpson, A. T., Spence, S. W. T., and Watterson, J. K., 2009. "A comparison of the flow structures and losses within vaned and vaneless stators for radial turbines". *Journal of Turbomachinery,* **131**.

[23] Galindo, J., Hoyas, S., Fajardo, P., and Navarro, R., 2013. "Set-up analysis and optimization of CFD simulations for radial turbines". *Engineering Applications of Computational Fluid Mechanics,* **7**(4), pp. 441–460.

[24] Terdich, N., 2015. "Impact of electrically assisted turbocharging on the transient response of an off-highway diesel engine". PhD thesis, Imperial College London.

[25] Borutzky, W., Barnard, B., and Thoma, J., 2002. "An orifice flow model for laminar and turbulent conditions". *Simulation Modelling Practice and Theory,* **10**(3), pp. 141–152.